Atypical viscous fracture of human femurs

Zohar Yosibash[a,*], Romina Plitman Mayo[a], Charles Milgrom[b]

[a] *Dept. of Mechanical Engineering, Ben-Gurion University of the Negev, Beer-Sheva 84105, Israel*

[b] *Hadassah Hospital, Ein-Kerem, Jerusalem, Israel*

Abstract

Creep phenomenon at the scale of bone tissue (small specimens) is known to be present and demonstrated for low strains. Here creep is demonstrated on a pair of fresh-frozen human femurs at the organ level at high strains. Under a constant displacement applied on femur's head, surface strains at the upper neck location increase with time until fracture, that occurs within 7-13 seconds. The monotonic increase in strains provides evidence on damage accumulation in the interior (probably damage to the trabeculae) prior to final fracture, a fact that hints on probable damage of the trabecular bone that occurs prior to the catastrophic fracture of the cortical surface layer.

Keywords: femur, fracture, creep

1. Introduction

Bone tissue exhibits both viscous effects as well as creep and stress relaxation Lakes et al. (1979). For example, several studies have been reported on the creep behavior of both trabecular and cortical bone tissue (for trabecular see Zilch et al. (1980); Bowman et al. (1994), and for cortical see Fondrk et al. (1988); Caler and Carter (1989)). Recent studies attempt to consider long-term bone creep effects to analyze the aseptic loosening of cemented

*Corresponding Author

Email address: zohary@bgu.ac.il (Zohar Yosibash)

prosthesis in femurs Norman et al. (2013) and creep phenomena in vertebral bones Luo et al.. The creep phenomenon is characterized by creep strain vs time curves that have three distinct regimes and by several possible power law relationships between applied stress, time-to-failure, and steady-state creep rate. Many of these relationships are similar to those for conventional engineering materials such as metals (tensile creep) and ceramics (compressive creep).

The viscous and creep effects are insignificant for short time scales in the orders of seconds and at moderately low strain levels. Therefore, patient-specific finite element (FE) models based on CT scans that become extensively popular for predicting the mechanical response and failure loads in long bones, disregard these time dependent effects and consider time-independent constitutive laws, see e.g. Keyak et al. (1990); Viceconti et al. (2004); Schileo et al. (2007); Bessho et al. (2007); Yosibash et al. (2007a,b); Trabelsi et al. (2009). In-vitro experiments aimed at validating the FE models are usually performed, during which fresh-frozen femurs are defrosted, instrumented by strain-gauges and loaded *monotonically* until fracture. Such experiments are inappropriate for the investigation of creep effects, and to the best of our knowledge the effect of creep on the fresh-frozen femur-level has not yet been investigated, especially at high strains. We here provide experimental evidence on the strong influence of creep leading to fracture (time-dependent) phenomena at the femur level. Furthermore, the creep effect at high strains may explain qualitatively the fracture initiation evolution, a topic which is under continuous debate and investigation.

2. Materials and Methods

A pair of femurs harvested from a 77 years old, 180cm high, 50kg Caucasian male donor, that deceased due to lung cancer, were deep-frozen after harvest and thawed at room temperature on the day of the experiment. Soft tissue was removed from the bone by a combination of sharp and blunt dissection. The femurs were then cut to about 250mm and the proximal parts were mounted into cylindrical steel devices. The mounting jig is documented in Yosibash et al. (2007a).

The left femur had a relatively medium sized tumor of the type adenocarcinoma in the head and lower part of the neck whereas the right femur had a very small tumor in the middle of the neck (determined by histopathology inspections after fracture).

Thirteen uniaxial strain gauges (SGs)(Vishay general purpose uniaxial SGs with a sensitivity of $\pm 0.2\%$) were bonded to the superior and inferior neck and the medial and lateral shaft, using M-Bond 200 Cyanoacrylate Adhesive (Measurements Group, Inc., Raleigh, NC, USA) (see SG distribution in Fig 1). The SGs were bonded so to align with the assumed local principal strain directions which could only be validated in a finite-element analysis at the post process phase. Three Vishay linear displacement sensors (LDS, precision of $\pm 0.2\%$) were used to measure displacements at two locations. Vishay system 7000 combined with Strain-Smart software was used to record the output data from the load cell (via an amplifier), SGs and LDS. The femurs were kept overnight in a humid container in a refrigerator until the next morning at which the mechanical experiments were performed.

A displacement driven compression machine Zwick 1445 (Zwick Gmbh

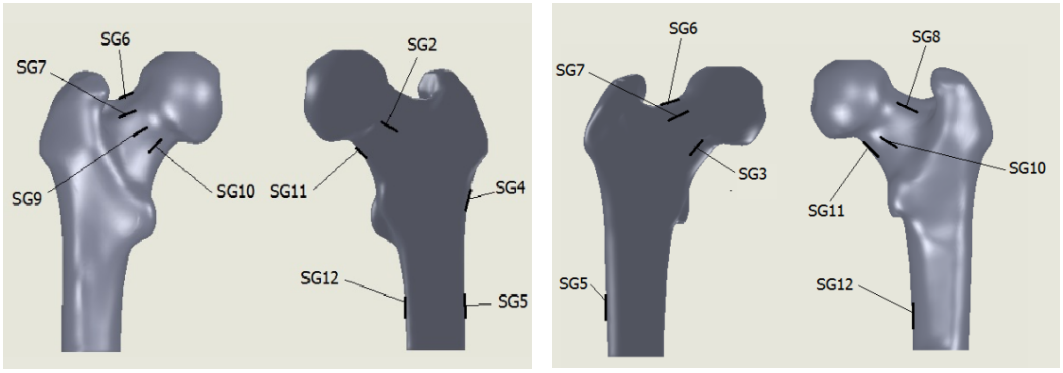

(a) Left Femur (b) Right Femur

Figure 1: The two proximal femurs and SGs locations.

& Co. KG., Germany 1992) was used that applied displacements at a rate of 16.67 mm/sec, while monitoring the load. A load cell with a saturation level of 12,000 Newton was used to measure the load. A flat and smooth aluminum plate applied the displacement directly to femur's head. Prior to the fracture experiment, loads of low magnitudes (up to 1000 N) were applied to the femurs at three inclination angles 0°, 7° and 15° which showed a linear response (SGs showed zero strains after removal of the load).

The femurs were finally inclined at 15° as shown in Figure 2, and a displacement on their head was applied.

The right femur's upper part of the head was subjected to a displacement of 3.7mm and the left femur to a displacement of 3.2mm (at a rate of 16.67 mm/sec) and then the displacement was kept constant until fracture.

Following fracture, a histopathology was performed to the broken heads to identify the metastatic tumors and their magnitude.

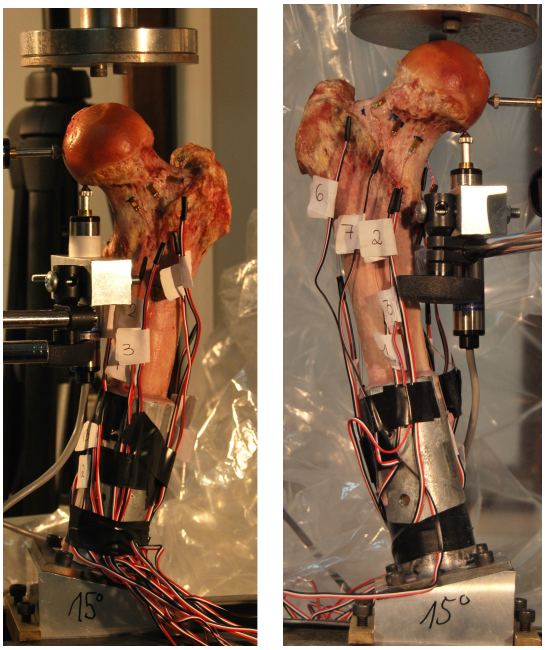

(a) Left Femur (b) Right Femur

Figure 2: The experimental setup.

3. Results

A transcervical fracture occurred in the left femur after 7.2 sec and a subcapital fracture in the right femur after 13.03 sec. The relevant SGs' output as a function of time (from the application of the displacement until fracture) is presented in Figure 3 for the left femur and in Figure 4 for the right femur.

The saturation level of the load cell is 12,000 N, so that applied displacement rate is terminated when this load is reached and thereafter the reached displacement (applied on the femurs' head) is kept constant. In Figure 5 we present the relative displacement (applied displacement over the maximum

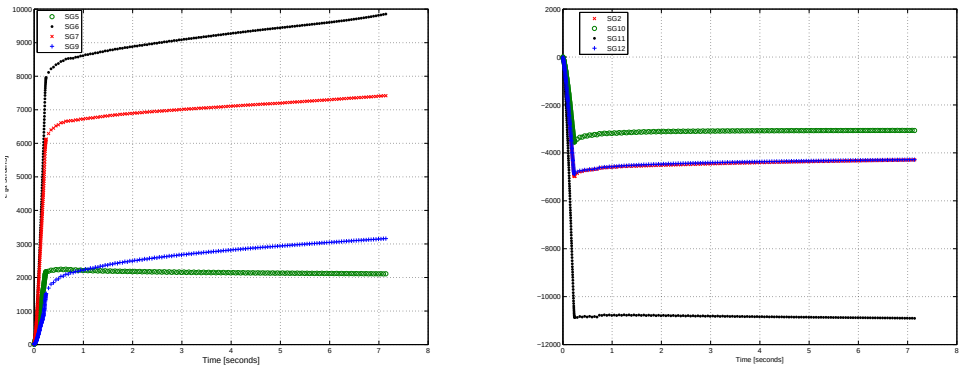

(a) SGs in Tension (b) SGs in Compression

Figure 3: Left femur: SG data (μstrains).

displacement) and the relative force on the right and left femurs as a function of time until fracture.

Figure 6 shows the the fractured femurs on which the mid-plane and histology with the tumor is superimposed.

The maximum strains (tension or compression) measured by the SGs at the neck are summarized in Tables 1-2.

Table 1: Strains in μstrains - Right femur

SG#	SG3	SG6	SG7	SG8	SG11
End elastic response$^{(1)}$	-2730	5492	3307	3735	-7749
Maximum	-3079$^{(2)}$	7545$^{(3)}$	5988$^{(4)}$	4253$^{(2)}$	-8581$^{(2)}$
Final (t=13.21s)	-2770	6992	5988	1928	-8003

(1) At t=0.23s, and load of [11706N], (2) Between t=0.23 and t=0.43, which is the time the load cell stop recording, (3) Between t=0.43 and fracture, (4) At fracture.

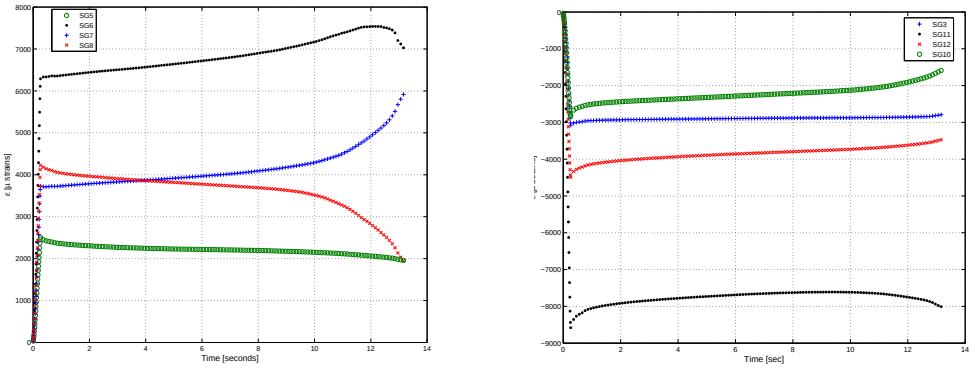

(a) SGs in Tension

(b) SGs in Compression

Figure 4: Right femur: SG data (μstrains).

Table 2: Strains in μstrains - Left femur

SG#	SG2	SG6	SG7	SG9	SG11
End elastic response$^{(1)}$	-4427	6614	5076	1038	-9446
Maximum	-4982$^{(2)}$	9873$^{(3)}$	7433$^{(3)}$	3175$^{(3)}$	-10918$^{(4)}$
Final (t=7.29s)	-4298	9862	7420	3154	-10916

(1) At t=0.20s, and load of [11749N], (2) Between t=0.20 and t=0.45, which is the time the load cell stop recording, (3) Between t=0.45 and fracture, (4) At fracture.

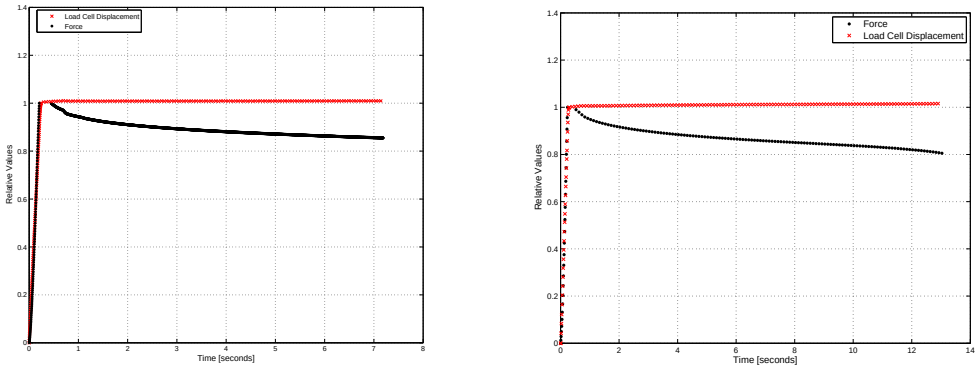

(a) Left Femur (b) Right Femur

Figure 5: Relative applied displacement and resulting load on the femurs.

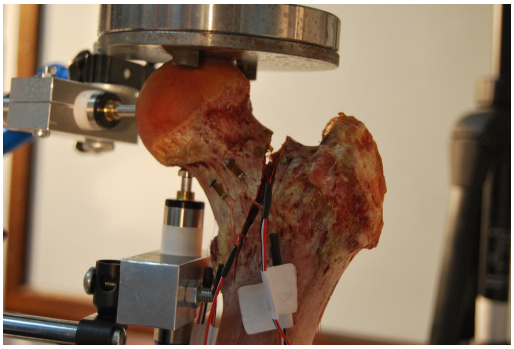

(a) Left Femur

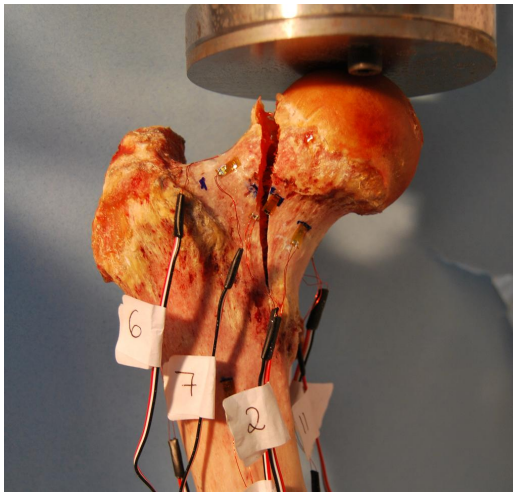

(b) Right Femur

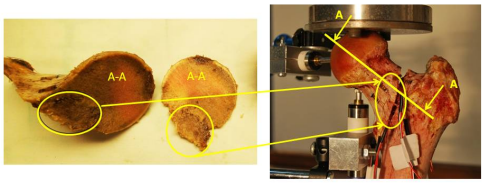

(c) Left - Fracture with tumor

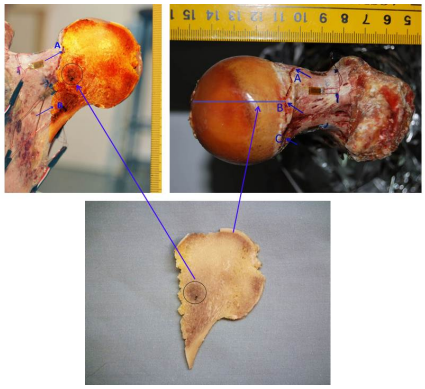

(d) Right - Fracture with tumor

Figure 6: The fractured femurs with location of tumor.

4. Discussion

Although the creep phenomenon is known to be present in bone tissues and demonstrated for low strains at the tissue level (relatively small extracted specimens), it is not investigated or demonstrated at the organ level, and its influence is mostly ignored. In this study we have shown that creep is clearly visible at the organ level at high strains in femurs. At a given constant displacement applied on the femur's head all measured strains change as a function of time, and the load decreases. The time to failure is relatively fast and occurs within 7-13 seconds. Since the experiments are displacement controlled, no visual evidence of the expected fracture is noticed until fracture.

Inspection of video films of the fracture process, and the SGs behavior as a function of time, provide evidence that in both femurs the fracture initiation occurs at the upper neck in tension. At this location the strain measured by SG6 (the closest SG to the anticipated starting point of the fracture on the surface) is the highest (among all other SGs) and increases as a function of time until fracture.

In the left femur, SG6 which is very close to the fracture path reaches almost 10,000 μstrains just before fracture, well beyond the anticipated "yield strain" of 7300 μstrain Bayraktar et al. (2004). In the right femur, SG6 although being the closest to the fracture initiation location, it is still further away and reaches 7500 μstrains just before fracture. The strain at the fracture location was not measured and is anticipated to be higher.

The fracture path is the typical path at which femurs, that are loaded in this configuration until fracture, break. The fracture path in the left femur is

a bit shifted from the head to the neck region - this may be attributed to the existence of a tumor of the type adenocarcinoma (determined by histology inspections after the test).

In the left femur the strains in the neck at the upper posterior location increase with time whereas in the right femur, the strains in the upper anterior location increase with time. The monotonic increase in strains on the surface provide evidence on damage accumulation in the interior (probably damage to the trabeculae) prior to final fracture, a fact that hints on probable damage of the trabecular bone that occurs prior to the catastrophic fracture of the cortical surface layer.

During the loading stage all SG respond linearly until the maximum load. This phenomenon suggests that at the macroscopic level no damage accumulation is visible if the femurs are loaded at a high strain rate monotonically until fracture, and they behave linearly elastic until fracture. This observation coincides with Juszczyk et al. (2011).

The limitations of the current study are: The maximum load was not measured due to the saturation level of the load cell at 12,000N. Tumors of the type adenocarcinoma are present (but very minor in the right femur) which may have an influence on the creep behavior.

Acknowledgement We would like to thank Dr. Nir Trabelsi from Shamun College of Engineering, Israel, Mr. Ilan Gilad and Mr. Natan Levin from the Ben-Gurion University, Israel, and Mr. Hagen Wille from TUM, Germany for their help with the experiments. The first author gratefully acknowledges the generous support of the Technical University of Munich - Institute for

Advanced Study, funded by the German Excellence Initiative. This study was supported in part by grant no. 3-00000-7375 from the Chief Scientist Office of the Ministry of Health, Israel.

References

Bayraktar, H., Morgan, E., Niebur, G., Morris, G., Wong, E., Keaveny, M., 2004. Comparison of the elastic and yield properties of human femoral trabecular and cortical bone tissue. Jour. Biomech. 37, 27–35.

Bessho, M., Ohnishi, I., Matsuyama, J., Matsumoto, T., Imai, K., Nakamura, K., 2007. Prediction of strength and strain of the proximal femur by a CT-based finite element method. Jour. Biomech. 40, 1745–1753.

Bowman, S.M., Keaveny, T., Gibson, J.L., Hayes, W., McMahon, T.A., 1994. Compressive creep behavior of bovine trabecula bone. Jour. Biomech. 27, 301–310.

Caler, W.E., Carter, D.R., 1989. Bone creep-fatigue damage accumulation. Jour. Biomech. 22, 625–635.

Fondrk, M., Bahniuk, E., Davy, D.T., Michaels, C., 1988. Some viscoplastic characteristics of bovine and human cortical bone. Jour. Biomech. 21, 623–630.

Juszczyk, M.M., Cristofolini, L., Viceconti, M., 2011. The human proximal femur behaves linearly elastic up to failure under physiological loading conditions. Jour. Biomech. 44, 2259–2266.

Keyak, J.H., Meagher, J.M., Skinner, H.B., Mote, J.C.D., 1990. Automated

three-dimensional finite element modelling of bone: A new method. ASME Jour. Biomech. Eng. 12, 389–397.

Lakes, R., Katz, J., Sternstein, S., 1979. Viscoelastic properties of wet cortical bone I. Torsional and biaxial studies. Jour. Biomech. 12, 657–678.

Luo, J., Pollintine, P., Gomm, E., Dolan, P., Adams, M.A., . Vertebral deformity arising from an accelerated "creep" mechanism. Eur. Spine Jour. .

Norman, T.L., Shultz, T., Noble, G., Gruen, T.A., Blaha, J.D., 2013. Bone creep and short and long term subsidence after cemented stem total hip arthroplasty (THA). Jour. Biomech. 46, 949–955.

Schileo, E., Taddei, F., Malandrino, A., Cristofolini, L., Viceconti, M., 2007. Subject-specific finite element models can accurately predict strain levels in long bones. Jour. Biomech. 40, 2982–2989.

Trabelsi, N., Yosibash, Z., Milgrom, C., 2009. Validation of subject-specific automated p-FE analysis of the proximal femur. Jour. Biomech. 42, 234–241.

Viceconti, M., Davinelli, M., Taddei, F., Cappello, A., 2004. Automatic generation of accurate subject-specific bone finite element models to be used in clinical studies. Jour. Biomech. 37, 1597–1605.

Yosibash, Z., Padan, R., Joscowicz, L., Milgrom, C., 2007a. A CT-based high-order finite element analysis of the human proximal femur compared to in-vitro experiments. ASME Jour. Biomech. Eng. 129, 297–309.

Yosibash, Z., Trabelsi, N., Milgrom, C., 2007b. Reliable simulations of the human proximal femur by high-order finite element analysis validated by experimental observations. Jour. Biomech. 40, 3688–3699.

Zilch, H., Rohlmann, A., Bergmann, G., Kolbel, R., 1980. Material properties of femoral cancellous bone in axial loading. Part II: Time dependent properties. Acta Orthop. Traumat. Surg. 97, 257–262.